Ultra-Low-Field MRI Enhancement via INR-Based Style Transfer

Kh Tohidul Islam[1 [0000−0003−2172−7041]], Mevan Ekanayake[1 [0000−0002−4768−5073]], and Zhaolin Chen[2 [0000−0002−0173−6090]]

[1] Monash Biomedical Imaging, Monash University, Clayton, VIC, Australia
[2] Department of Data Science and AI, Monash University, Clayton, VIC, Australia
{KhTohidul.Islam,Mevan.Ekanayake,Zhaolin.Chen}@monash.edu

Abstract. Ultra-low-field (ULF) Magnetic Resonance Imaging (MRI) improves accessibility and affordability but suffers from lower image quality compared to high-field MRI. This study proposes a novel enhancement framework that integrates Implicit Neural Representations (INRs) with Neural Style Transfer (NST) to improve ULF MRI quality by transferring high-resolution structural details from 7T MRI. Unlike conventional methods, our approach does not require paired datasets or extensive pre-training, leveraging INR's continuous representation and NST's perceptual refinement to enhance contrast, sharpness, and noise suppression. Quantitative evaluations on T1-weighted ULF MRI demonstrate significant improvements in perceptual quality (PIQE), contrast-to-noise ratio (CNR), and structural consistency (MLC/MSLC), outperforming state-of-the-art methods. These findings underscore the potential of INR-driven learning for advancing MRI reconstruction, enabling higher-quality imaging in resource-limited settings. Our method is fully unsupervised and operates in an unpaired setting, requiring no voxel-wise correspondence or labeled training data. The implementation of our proposed method and model hyperparameters is publicly available at https://github.com/khtohidulislam/ULF-MRI-Enhance.

Keywords: Ultra-low-field MRI · High-field MRI · Image Quality Enhancement · Implicit Neural Representations · Neural Style Transfer.

1 Introduction and Background

Magnetic Resonance Imaging (MRI) is a cornerstone of non-invasive diagnostic imaging, offering detailed insights into anatomical and functional structures. However, image quality in MRI is largely dictated by field strength, where high-field systems ($\geq 1T$) provide superior spatial resolution, tissue contrast, image uniformity, and signal-to-noise ratios (SNR) but are constrained by high costs, scanner availability, infrastructure demands, and limited accessibility [22,1,2,28].

Ultra-low-field (ULF) MRI ($< 0.1T$) offers a cost-effective and portable alternative, expanding accessibility to under-resourced and point-of-care settings [5,13,10,18,12,21]. However, its clinical utility is hindered by inherently low SNR,

poor contrast resolution, and increased noise, particularly affecting gray and white matter differentiation [4,15]. Traditional hardware-based solutions, such as stronger gradient coils, advanced signal processing, or improved RF technology, are often impractical due to cost and operational constraints, necessitating computational approaches for image quality enhancement [19,16].

Recent advances in deep learning have shown promise in mitigating these limitations. Unsupervised denoising methods such as Neighbor2Neighbor (N2N) [9], DIP [26], and Noise2Void [17] enhance image quality without requiring clean-noisy pairs, leveraging self-supervision from noisy images. However, these approaches often struggle with preserving high-frequency details in medical images.

Implicit Neural Representations (INRs) have emerged as a promising architecture, modeling images as continuous functions over spatial coordinates. SIREN [25] demonstrated the effectiveness of periodic activation functions in representing fine-grained textures, while subsequent extensions, such as DINER and WIRE, improved resolution and contrast via disorder-invariant modeling, hierarchical representations, and wavelet representations [27,23]. Unlike DINER or WIRE, which are optimized for natural images, our method is inspired by emerging medical INR applications, adapted for subject-level MRI enhancement without supervision or paired data.

Neural Style Transfer (NST) has further introduced a complementary avenue by enabling the transfer of stylistic and structural features from high-field MRI to ULF scans. Originally developed for artistic applications [8,14], NST has been explored in medical imaging for harmonizing contrast and enhancing texture detail [24]. However, its direct application remains limited due to challenges in maintaining anatomical fidelity and suppressing artifacts.

To address these limitations, we propose a novel INR-based enhancement framework integrated with NST to elevate ULF MRI quality (Figure 1). Our approach leverages residual SIREN models for high-fidelity, continuous spatial representation while integrating NST to transfer high-field MRI features without requiring paired datasets. This synergy allows our method to enhance contrast, suppress noise, and preserve anatomical structures more effectively than existing approaches, surpassing state-of-the-art methods perceptually and quantitatively.

2 Method

Our framework integrates an enhanced SIREN-based implicit neural representations Framework (INR) model with residual connections to reconstruct ultra-low-field (ULF) MRI images with high fidelity. INRs parameterize images as continuous functions $f_\theta : \mathbb{R}^2 \to \mathbb{R}$, where each spatial coordinate (x, y) is mapped to an intensity value. This continuous representation enables arbitrary-resolution synthesis, facilitating high-frequency detail preservation, noise suppression, contrast enhancement, and structural consistency while improving perceptual fidelity.

Unlike traditional convolutional models, our approach leverages periodic activation functions to efficiently encode fine anatomical structures while maintaining smooth spatial continuity. The architecture consists of an initial linear

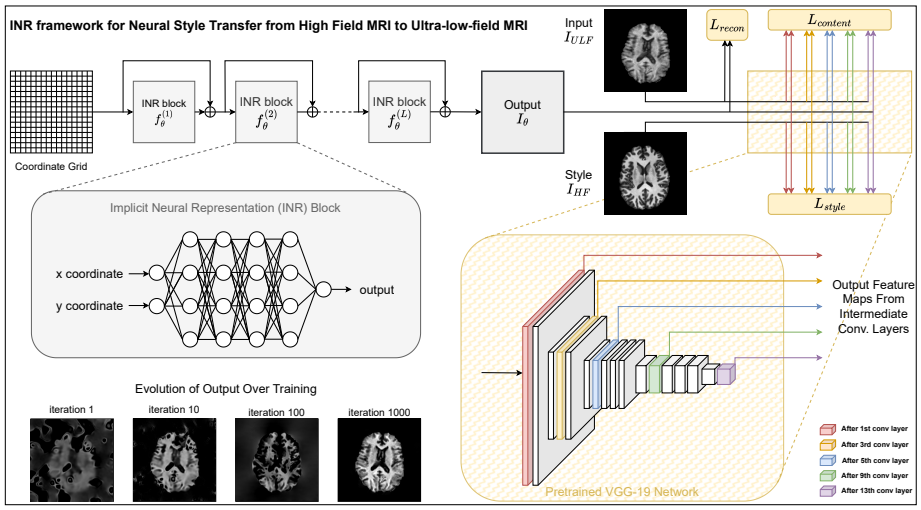

Fig. 1. The proposed framework for enhancing ULF MRI quality via INR and NST.

projection, followed by multiple residual SIREN blocks, and a final output layer. Each residual block contains 256 neurons with sinusoidal activations, ensuring stable feature propagation and effective learning of high-frequency textures. To improve model convergence, we employ spectral bias mitigation through a tailored weight initialization scheme, as proposed in [25].

Formally, an MRI image I is modeled as a function $f_\theta : \mathbb{R}^2 \to \mathbb{R}$, where θ represents the trainable parameters. Given a low-field MRI image $I_{ULF} \in \mathbb{R}^{W_0 \times H_0}$ and a high-field reference $I_{HF} \in \mathbb{R}^{W_0 \times H_0}$, our objective is to reconstruct a high-quality approximation $\hat{I}_{ULF}$ such that:

$$\hat{I}_{ULF}(x, y) = f_\theta(x, y), \quad \text{where} \quad f_\theta = \arg\min_\theta \mathcal{L}_{\text{total}}(I_{ULF}, I_{HF}). \tag{1}$$

The total loss function $\mathcal{L}_{\text{total}}$ is designed to optimize perceptual quality, contrast, structural fidelity, and texture consistency, incorporating content, style, edge preservation, and reconstruction constraints.

Theoretical foundation of INR-Based Style Transfer: The effectiveness of our INR-based enhancement is supported by the properties of sinusoidal activation functions, Gram matrix-based style transfer, and residual connections. They collectively ensure robust high-field contrast adaptation while preserving fine anatomical structures,

1. *Spectral Bias Mitigation*: The use of sinusoidal activations enables INR models to capture high-frequency image details while avoiding over-smoothing, ensuring accurate representation of fine anatomical structures [25].

2. *Feature Matching via Gram Matrices*: The style loss minimizes the discrepancy between Gram matrices of deep VGG features extracted from I_θ and I_{HF}, enforcing perceptual consistency across multiple resolution scales.
3. *Residual Connections for Stability*: The incorporation of residual SIREN blocks ensures stable optimization, preventing the loss of spatial coherence while facilitating high-contrast adaptation.

These components collectively ensure that the learned function f_θ converges to a solution that balances fine-detail preservation with high-field contrast adaptation, effectively bridging the quality gap between ULF and high-field MRI.

Neural Style Transfer for High-Field Contrast Adaptation To guide the enhancement process, we define a total loss function balancing content, style, and reconstruction objectives. The content loss preserves anatomical structures by minimizing feature discrepancies between the enhanced image I_θ and the ULF input I_{ULF}. The style loss ensures high-field contrast adaptation by aligning Gram matrices of deep VGG feature representations from I_θ and I_{HF}. Additionally, a reconstruction loss constrains I_θ to maintain structural coherence with I_{ULF}, preventing excessive texture hallucination. The final optimization objective is:

$$L_{\text{total}} = \alpha L_{\text{content}} + \beta L_{\text{style}} + \gamma L_{\text{recon}}. \tag{2}$$

The trained INR model then parameterizes the enhanced image as a continuous function $I_\theta(x, y) = f_\theta(x, y)$, allowing high-resolution synthesis at arbitrary scales. Unlike conventional super-resolution models, our approach inherently preserves fine anatomical details and adapts resolution dynamically to clinical needs.

Residual INR with Multi-Resolution Encoding A key advantage of our framework is its multi-resolution feature matching capability, which facilitates contrast harmonization without requiring voxel-wise correspondences. This is achieved by computing the style loss at multiple scales using deep VGG feature representations, ensuring perceptual consistency across anatomical structures. Additionally, residual INR blocks improve information flow during training, mitigating vanishing gradients and enabling stable optimization.

The forward pass in a residual SIREN block can be expressed as:

$$f_\theta^{(l+1)}(x, y) = f_\theta^{(l)}(x, y) + \sigma(W^{(l)} f_\theta^{(l)}(x, y) + b^{(l)}) \tag{3}$$

where $\sigma(\cdot)$ is the sinusoidal activation, and $W^{(l)}, b^{(l)}$ are the learnable weights and biases of layer l. This residual formulation ensures that high-frequency features are not attenuated during training, leading to sharper reconstructions.

To further improve robustness, we introduce a spectral bias mitigation strategy that ensures high-frequency details are effectively captured. This prevents texture oversmoothing, a common issue in standard deep learning-based MRI enhancement methods. Supervised methods typically rely on paired or multi-contrast training data, which are not available for 64mT T1-weighted MRI.

Therefore, we focus on unsupervised strategies compatible with the constraints of our imaging setup. Unlike conventional CNN-based super-resolution models, which rely on discrete convolutions and fixed receptive fields, our approach leverages a continuous representation, enabling arbitrary-resolution synthesis, finer structural preservation, and improved anatomical coherence.

3 Experiments and Results

This study was approved by the Monash University, Australia, Research Ethics Committee, with informed consent obtained from all participants. We used T1-weighted MRI scans from two sources: ULF images acquired with the Hyperfine Swoop system at 64mT, processed with skull stripping and isotropic resampling to 1 mm^3 resolution, and high-field 7T images from a Siemens Magnetom scanner [3], co-registered to the ULF scans. The superior resolution and contrast of 7T MRI serve as a reference for unpaired style transfer, allowing our framework to enhance ULF images without requiring voxel-wise correspondences [11].

We validate our proposed method through quantitative and qualitative assessments, comparing enhanced 64mT MRI images with high-field 7T MRI references. The implicit neural representation (INR) model, f_θ, is a five-layer fully connected network with 128 neurons per layer, leveraging sinusoidal activations with a frequency parameter of $\omega = 30$ [25]. The model was optimized using the Adam optimizer ($\text{lr} = 1 \times 10^{-4}$) over 1,000 iterations, minimizing the weighted sum of content, style, and reconstruction losses ($\alpha = 3$, $\beta = 15$, $\gamma = 1$). Experiments were conducted on a NVIDIA A40 GPU.

3.1 Image Quality Assessment

Standard full-reference metrics (e.g., SSIM, PSNR, LPIPS) are not applicable in our unpaired setting due to lack of voxel-wise correspondence. We therefore adopt a multi-faceted assessment strategy encompassing both perceptual and structural consistency metrics to evaluate the enhancement of ULF MRI images. These include the Perception-based Image Quality Evaluator (PIQE) for no-reference image quality estimation, Contrast-to-Noise Ratio (CNR) for contrast differentiation, and two structural correlation measures—Mean Line Correlation (MLC) and Mean Shifted Line Correlation (MSLC), to quantify local and global consistency, spatial coherence, and edge preservation [6].

PIQE: Perceptual Image Quality Estimation PIQE provides a no-reference image quality assessment by quantifying distortions related to sharpness, noise, texture, artifacts, structural integrity, and perceptual fidelity. It is computed as:

$$\text{PIQE} = w_1 \cdot \overline{\sigma^2} + w_2 \cdot \overline{C} + w_3 \cdot \sigma_{\text{noise}}, \tag{4}$$

where $\overline{\sigma^2}$ represents the average local variance, $\overline{C}$ denotes the mean contrast across image patches, and σ_{noise} corresponds to the estimated noise level.

CNR: Contrast Differentiation CNR quantifies the ability to distinguish between anatomical structures of varying intensities while accounting for background noise, signal uniformity, tissue contrast, and diagnostic clarity:

$$CNR = \frac{\Delta S}{\sigma_{\text{noise}}}, \tag{5}$$

where ΔS is the intensity difference between segmented gray and white matter regions, and σ_{noise} represents the standard deviation of background noise.

MLC: Local Structural Consistency MLC evaluates the correlation between adjacent rows and columns, reflecting local image consistency and suppression:

$$\text{MLC} = \frac{1}{N}\sum_{i=1}^{N} \rho(\text{row}_i, \text{row}_{i+1}) + \rho(\text{col}_i, \text{col}_{i+1}), \tag{6}$$

where ρ is the Pearson correlation between neighboring pixels, and N denotes the total number of rows and columns.

MSLC: Global Structural Detail Preservation MSLC captures large-scale structural coherence by measuring correlation between spatially distant rows and columns:

$$\text{MSLC} = \frac{1}{M}\sum_{i=1}^{M} \rho(\text{row}_i, \text{row}_{i+\frac{H}{2}}) + \rho(\text{col}_i, \text{col}_{i+\frac{W}{2}}), \tag{7}$$

where ρ denotes the Pearson correlation, M is the number of sampled row-column pairs, and H, W correspond to image height and width.

3.2 Quantitative Evaluation

We assessed image enhancement on 50 ULF MRI scans across 8,000 axial slices (224×224 resolution) using PIQE, CNR, MLC, and MSLC (Table 1). PIQE decreased significantly (↓), indicating improved perceptual quality. CNR (with gray and white matter segmented using FAST in FSL [20,7]) increased (↑), demonstrating enhanced contrast between gray and white matter. MLC was highest for our method, reflecting better local consistency. MSLC was lowest for our method, preserving structural details while mitigating over-smoothing. Compared to N2N [9] and SIREN [25], our approach achieved a better balance between noise suppression and structural detail retention.

3.3 Qualitative Evaluation

Figure 2 visually compares enhancement results across different methods, with 7T MRI images as unpaired high-field references. Our method preserves anatomical structures, reduces noise, and enhances the contrast between gray and white matter, outperforming N2N and SIREN in structural clarity. This aligns with our quantitative findings.

Table 1. Comparative Analysis of Image Quality Metrics Following Enhancement.

Method	PIQE (↓)	CNR (↑)	MLC (↑)	MSLC (↓)
Baseline (64mT MRI)	67.41 ± 5.30	3.00 ± 0.20	0.9761 ± 0.0045	0.6024 ± 0.035
N2N [9]	65.01 ± 5.28	2.93 ± 0.40	0.9829 ± 0.0038	0.6260 ± 0.029
SIREN [25]	72.05 ± 4.85	3.15 ± 0.65	0.9781 ± 0.0052	0.6107 ± 0.032
Ours	$\mathbf{50.71 \pm 4.83}$	$\mathbf{5.01 \pm 0.32}$	$\mathbf{0.9874 \pm 0.0032}$	$\mathbf{0.2090 \pm 0.018}$

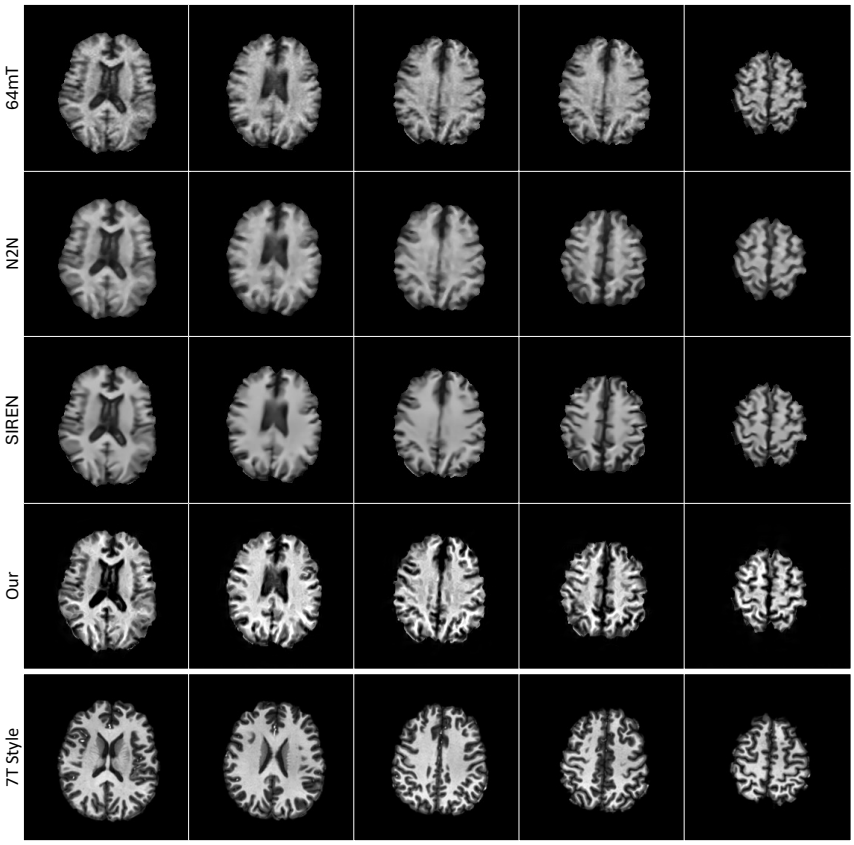

Fig. 2. Comparative visualization of image enhancement methods on ULF MRIs.

3.4 Regional Analysis: ROI Comparisons

To further evaluate structural preservation, we extracted and upscaled two regions of interest (ROIs) (red and blue) across all methods. Our approach maintains sharper edges and finer structural details while suppressing noise, suggesting superior preservation of tissue boundaries (Figure 3(A)). Additionally, we incorporated scatter plots, (Figure 3(B)), comparing contrasts between CSF to GM, and CSF to WM, further demonstrating the enhanced contrast preservation of our method in differentiating these tissue types.

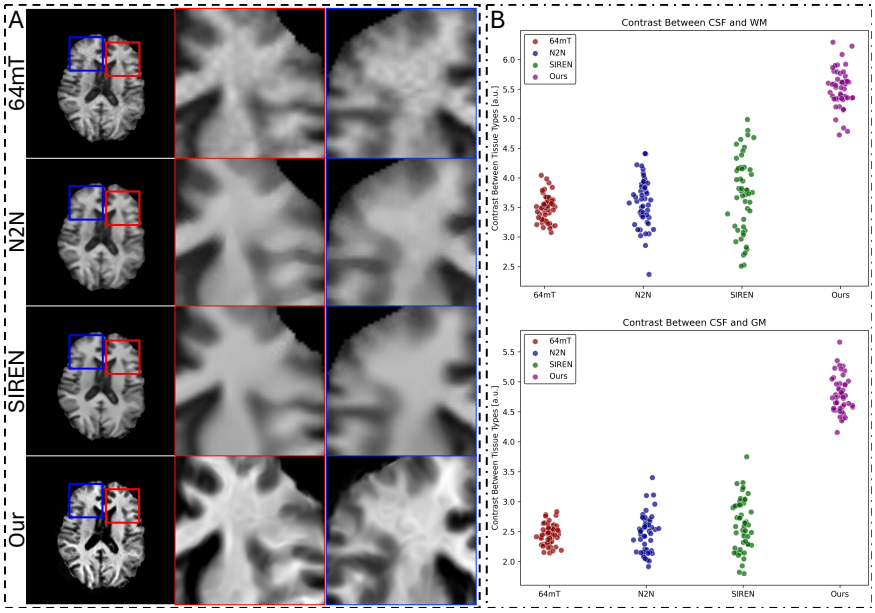

Fig. 3. Comparison of two ROIs (A) extracted and upscaled, highlighting differences in structural detail, edge sharpness, and noise reduction. Scatter plots (B) for contrasts between CSF to GM and CSF to WM, respectively, across all datasets.

3.5 Ablation Study:

We evaluated six configurations (Table 2): (1) Baseline (64mT MRI), (2) NST only, (3) INR only, (4) INR + NST (Shallow VGG: conv1_1, conv2_1), (5) INR + NST (Mid-Level VGG: conv1_1 to conv4_1), and (6) INR + NST (Full VGG: conv1_1 to conv5_1). NST alone improves perceptual quality (lower PIQE) but struggles with structural preservation (higher MSLC), while INR enhances local consistency (higher MLC) but lacks contrast enhancement (lower CNR). Combining INR and NST progressively improves all metrics, with deeper VGG features further enhancing contrast, edge sharpness, and structure retention. The full VGG configuration achieves the best overall performance, highlighting the importance of multi-scale feature extraction in MRI enhancement.

Table 2. Ablation Study on the Impact of INR, NST, and VGG Feature Selection.

Configuration	PIQE (↓)	CNR (↑)	MLC (↑)	MSLC (↓)
Baseline (64mT MRI)	67.41 ± 5.30	3.00 ± 0.20	0.9761 ± 0.0045	0.6024 ± 0.035
NST Only	60.92 ± 5.10	3.71 ± 0.38	0.9786 ± 0.0037	0.5703 ± 0.031
INR Only	61.23 ± 5.18	3.42 ± 0.35	0.9805 ± 0.0039	0.5802 ± 0.032
INR + NST (Shallow VGG)	58.77 ± 5.02	3.85 ± 0.28	0.9828 ± 0.0036	0.5405 ± 0.030
INR + NST (Mid-Level VGG)	54.91 ± 4.95	4.42 ± 0.34	0.9852 ± 0.0034	0.3809 ± 0.025
INR + NST (Full VGG)	$\mathbf{50.71 \pm 4.83}$	$\mathbf{5.01 \pm 0.32}$	$\mathbf{0.9874 \pm 0.0032}$	$\mathbf{0.2090 \pm 0.018}$

4 Conclusions

This work introduces an INR-NST framework to enhance ULF MRI by transferring high-field features, improving contrast, sharpness, and noise reduction without requiring paired datasets or extensive pre-training. Quantitative evaluations demonstrate superior perceptual quality, contrast, and structural consistency over existing methods like N2N and SIREN. The unpaired and fully unsupervised nature of our framework makes it particularly suitable for low-resource imaging settings such as 64mT MRI. While effective, our approach incurs increased training and inference time due to deep feature extraction and residual blocks, with potential sensitivity to high-field style selection. Future work will explore 3D extensions and task-aware priors to enhance generalization across MRI contrasts and scanner variations, further advancing INR-driven solutions for robust and scalable ULF MRI enhancement.

Acknowledgments. This research receives funding from the National Imaging Facility (NIF), Australia, and Hyperfine Inc. The authors acknowledge the facilities and scientific and technical assistance of the NIF, a National Collaborative Research Infrastructure Strategy capability, at the Monash Biomedical Imaging, Monash University.

Disclosure of Interests. The authors declare no competing interests.

References

1. Arnold, T.C., Freeman, C.W., Litt, B., Stein, J.M.: Low-field MRI: Clinical promise and challenges. Journal of Magnetic Resonance Imaging **57**(1), 25–44 (Jan 2023). https://doi.org/10.1002/jmri.28408
2. Campbell-Washburn, A.E., Keenan, K.E., Hu, P., et al.: Low-field MRI: A report on the 2022 ISMRM workshop. Magnetic Resonance in Medicine **90**(4), 1682–1694 (Jun 2023). https://doi.org/10.1002/mrm.29743
3. Chen, X., Qu, L., Xie, Y., et al.: A paired dataset of T1- and T2-weighted MRI at 3 Tesla and 7 Tesla. Scientific Data **10**(1), 489 (Jul 2023). https://doi.org/10.1038/s41597-023-02400-y
4. Deoni, S.C., Bruchhage, M.M., Beauchemin, J., et al.: Accessible pediatric neuroimaging using a low field strength MRI scanner. NeuroImage **238**, 118273 (Sep 2021). https://doi.org/10.1016/j.neuroimage.2021.118273
5. DesRoche, C.N., Johnson, A.P., Hore, E.B., et al.: Feasibility and Cost Analysis of Portable MRI Implementation in a Remote Setting in Canada. Canadian Journal of Neurological Sciences p. 1–10 (Jul 2023). https://doi.org/10.1017/cjn.2023.250
6. Dohmen, M., Klemens, M.A., Baltruschat, I.M., Truong, T., Lenga, M.: Similarity and quality metrics for mr image-to-image translation. Scientific Reports **15**(1) (Jan 2025). https://doi.org/10.1038/s41598-025-87358-0
7. Fushimi, Y., Miki, Y., Urayama, S.i., et al.: Gray matter-white matter contrast on spin-echo T1-weighted images at 3 T and 1.5 T: a quantitative comparison study. European Radiology **17**(11), 2921–2925 (Jul 2007). https://doi.org/10.1007/s00330-007-0688-9

8. Gatys, L.A., Ecker, A.S., Bethge, M.: Image Style Transfer Using Convolutional Neural Networks. In: 2016 IEEE Conference on Computer Vision and Pattern Recognition (CVPR). pp. 2414–2423. IEEE, Las Vegas, NV, USA (Jun 2016). https://doi.org/10.1109/CVPR.2016.265
9. Huang, T., Li, S., Jia, X., Lu, H., Liu, J.: Neighbor2Neighbor: Self-Supervised Denoising from Single Noisy Images. In: 2021 IEEE/CVF Conference on Computer Vision and Pattern Recognition (CVPR). pp. 14776–14785. IEEE, Nashville, TN, USA (Jun 2021). https://doi.org/10.1109/CVPR46437.2021.01454
10. Iglesias, J.E., Schleicher, R., Laguna, S., et al.: Quantitative Brain Morphometry of Portable Low-Field-Strength MRI Using Super-Resolution Machine Learning. Radiology **306**(3) (Mar 2023). https://doi.org/10.1148/radiol.220522
11. Isaacs, B.R., Mulder, M.J., Groot, J.M., et al.: 3 versus 7 Tesla magnetic resonance imaging for parcellations of subcortical brain structures in clinical settings. PLOS ONE **15**(11), e0236208 (Nov 2020). https://doi.org/10.1371/journal.pone.0236208
12. Islam, K.T., Zhong, S., Zakavi, P., et al.: Improving portable low-field mri image quality through image-to-image translation using paired low- and high-field images. Scientific Reports **13**(1) (Dec 2023). https://doi.org/10.1038/s41598-023-48438-1
13. Islam, O., Lin, A.W., Bharatha, A.: Potential application of ultra-low field portable MRI in the ICU to improve CT and MRI access in Canadian hospitals: a multicenter retrospective analysis. Frontiers in Neurology **14** (Sep 2023). https://doi.org/10.3389/fneur.2023.1220091
14. Johnson, J., Alahi, A., Fei-Fei, L.: Perceptual Losses for Real-Time Style Transfer and Super-Resolution. In: ECCV 2016, vol. 9906, pp. 694–711. Springer International Publishing, Amsterdam, The Netherlands (2016). https://doi.org/10.1007/978-3-319-46475-6_43
15. Kimberly, W.T., Sorby-Adams, A.J., Webb, A.G., et al.: Brain imaging with portable low-field mri. Nature Reviews Bioengineering **1**(9), 617–630 (Jul 2023). https://doi.org/10.1038/s44222-023-00086-w
16. Koonjoo, N., Zhu, B., Bagnall, G.C., Bhutto, D., Rosen, M.S.: Boosting the signal-to-noise of low-field MRI with deep learning image reconstruction. Scientific Reports **11**(1) (Apr 2021). https://doi.org/10.1038/s41598-021-87482-7
17. Krull, A., Buchholz, T.O., Jug, F.: Noise2Void - Learning Denoising From Single Noisy Images. In: 2019 IEEE/CVF Conference on Computer Vision and Pattern Recognition (CVPR). pp. 2124–2132. IEEE, Long Beach, CA, USA (Jun 2019). https://doi.org/10.1109/CVPR.2019.00223
18. Lau, V., Xiao, L., Zhao, Y., et al.: Pushing the limits of low-cost ultra-low-field mri by dual-acquisition deep learning 3D superresolution. Magnetic Resonance in Medicine **90**(2), 400–416 (Apr 2023). https://doi.org/10.1002/mrm.29642
19. Lin, H., Figini, M., Tanno, R., et al.: Deep Learning for Low-Field to High-Field MR: Image Quality Transfer with Probabilistic Decimation Simulator. In: Machine Learning for Medical Image Reconstruction. pp. 58–70. Lecture Notes in Computer Science, Springer International Publishing, Shenzhen, China (2019). https://doi.org/10.1007/978-3-030-33843-5_6
20. Manson, E.N., Inkoom, S., Mumuni, A.N., et al.: Assessment of the Impact of Turbo Factor on Image Quality and Tissue Volumetrics in Brain Magnetic Resonance Imaging Using the Three-Dimensional T1-Weighted (3D T1W) Sequence. International Journal of Biomedical Imaging **2023**, 1–9 (Nov 2023). https://doi.org/10.1155/2023/6304219
21. Okar, S.V., Nair, G., Kawatra, K.D., Thommana, A.A., Donnay, C.A., Gaitán, M.I., Stein, J.M., Reich, D.S.: High-Field-Blinded Assessment of Portable Ultra-

Low-Field Brain MRI for Multiple Sclerosis. Journal of Neuroimaging **35**(1) (Jan 2025). https://doi.org/10.1111/jon.70005
22. Pogarell, T., Heiss, R., Janka, R., et al.: Modern low-field MRI. Skeletal Radiology (Feb 2024). https://doi.org/10.1007/s00256-024-04597-4
23. Saragadam, V., LeJeune, D., Tan, J., et al.: WIRE: Wavelet Implicit Neural Representations. In: 2023 IEEE/CVF Conference on Computer Vision and Pattern Recognition (CVPR). pp. 18507–18516. IEEE, Vancouver, BC, Canada (Jun 2023). https://doi.org/10.1109/CVPR52729.2023.01775
24. Shen, G., Zhu, Y., Jara, H., et al.: MRI Field-transfer Reconstruction with Limited Data: Regularization by Neural Style Transfer (2023). https://doi.org/10.48550/ARXIV.2308.10968
25. Sitzmann, V., Martel, J.N.P., Bergman, A.W., et al.: Implicit Neural Representations with Periodic Activation Functions. In: Proceedings of NIPS. pp. 7462–7473. NIPS'20, Curran Associates Inc., Red Hook, NY, USA (Dec 2020), https://dl.acm.org/doi/10.5555/3495724.3496350
26. Ulyanov, D., Vedaldi, A., Lempitsky, V.: Deep Image Prior. International Journal of Computer Vision **128**(7), 1867–1888 (Jul 2020). https://doi.org/10.1007/s11263-020-01303-4
27. Xie, S., Zhu, H., Liu, Z., et al.: DINER: Disorder-Invariant Implicit Neural Representation. In: 2023 IEEE/CVF Conference on Computer Vision and Pattern Recognition (CVPR). pp. 6143–6152. IEEE, Vancouver, BC, Canada (Jun 2023). https://doi.org/10.1109/CVPR52729.2023.00595
28. Zhao, Y., Ding, Y., Lau, V., Man, C., Su, S., Xiao, L., Leong, A.T.L., Wu, E.X.: Whole-body magnetic resonance imaging at 0.05 Tesla. Science **384**(6696) (May 2024). https://doi.org/10.1126/science.adm7168